

# Cytoplasmic streaming in plant cells emerges naturally by microfilament self-organization

Francis G. Woodhouse and Raymond E. Goldstein<sup>1</sup>

Department of Applied Mathematics and Theoretical Physics, University of Cambridge, Cambridge CB3 0WA, United Kingdom

Edited by T. C. Lubensky, University of Pennsylvania, Philadelphia, PA, and approved July 8, 2013 (received for review February 13, 2013)

Many cells exhibit large-scale active circulation of their entire fluid contents, a process termed cytoplasmic streaming. This phenomenon is particularly prevalent in plant cells, often presenting strikingly regimented flow patterns. The driving mechanism in such cells is known: myosin-coated organelles entrain cytoplasm as they process along actin filament bundles fixed at the periphery. Still unknown, however, is the developmental process that constructs the well-ordered actin configurations required for coherent cell-scale flow. Previous experimental works on streaming regeneration in cells of Characean algae, whose longitudinal flow is perhaps the most regimented of all, hint at an autonomous process of microfilament self-organization driving the formation of streaming patterns during morphogenesis. Working from first principles, we propose a robust model of streaming emergence that combines motor dynamics with both microscopic and macroscopic hydrodynamics to explain how several independent processes, each ineffectual on its own, can reinforce to ultimately develop the patterns of streaming observed in the Characeae and other streaming species.

cyclosis | *Chara* | active matter

Cytoplasmic streaming pervades the vast spectrum of cell types, achieving great diversity to fulfill many varied goals. *Drosophila* oocytes use disorderly streaming to localize proteins without counterproductive backflows (1, 2); *Caenorhabditis elegans* couples cortical flow with bistable pattern formation for polarity determination (3); *Elodea* leaf cells circulate chloroplasts in response to illumination (4); and pollen tubes transport tip growth material in fountain-like flows (5, 6), to name four disparate examples. At their core, either as the end goal or within the mechanism itself, lies the biological pillar of pattern formation (7).

The different realizations of streaming can be effectively categorized by the degree of order inherent in the observed flow (4, 8). The most disordered instances often function as part of cellular patterning processes, as in *Drosophila*. In contrast, the orderly types must themselves already be the product of some pattern-forming process to exist at all. The basic paradigm that underlies streaming, motor proteins interacting with polymer filaments, has been seen to possess many pattern-forming behaviors in both theoretical (9–11) and experimental (11–14) settings, with recent work beginning to incorporate the effects of cylindrical cell-like domains (15, 16). However, such studies are often “bottom up,” taken out of context from concrete biological systems, and in particular no direct connection has been made to the development of cytoplasmic streaming.

If we want to understand what fundamental dynamics drive the formation of orderly streaming and connect the microscopic with the macroscopic, an alternative “top-down” approach is warranted. To this end, we approach the problem by way of a concrete, prototype system. We adopt perhaps the most strikingly patterned example of all, the aquatic alga *Chara corallina* (Fig. 1A). The giant cylindrical internodal cells of *Chara* measure 1 mm in diameter and up to 10 cm in length. First observed in 1774 (17), its rotational streaming—termed “cyclosis”—is driven by vesicles (in the endoplasmic reticulum) coated with the motor

protein myosin (18–20) sliding along two oppositely directed longitudinal stripes of many continuous, parallel actin filament cables (21, 22) (Fig. 1B and C). Every cable is a bundle of many individual actin filaments, each possessing the same intrinsic polarity (23); myosin motors walk on a filament in a directed fashion, from its minus (pointed) end to its plus (barbed) end. These cables are bound to the cortically fixed chloroplasts at the cell periphery (24) in a “barber pole” twist, generating flow speeds of 50–100  $\mu\text{m/s}$  (25–27). It is unclear how this simple yet striking pattern forms during morphogenesis; what process is responsible for forming two, and only two, precisely equal stripes? One could imagine it to be the result of complex chemical pre-patterning, but experimental evidence suggests otherwise.

Foissner and Wasteneys (28) introduced the agents cytochalasin D and oryzalin into young *Chara* cells to arrest streaming and completely disorganize the established actin cables. They found a gradual recovery process (Fig. 2) whereby streaming initially resumes in a disordered saltatory fashion. Over time, the filaments reorganize, first into locally ordered “streamlets,” until eventually the initial filament layout is reestablished. They note one crucial difference from the prearrest configuration: the so-called indifferent zone (IZ) (Fig. 1B) separating the up- and down-streaming stripes, initially identifiable by a line of missing chloroplasts, is often found in a new position. Put another way, the entire pattern has shifted around the central axis. Together with the local-to-global progression, also observed in other cell types (8, 29), a self-organization process is implicated.

Similar behavior has been induced in rotationally streaming *Vallisneria* leaf cells where flow handedness was preserved only if some “seed” filament bundles survived disintegration (30), a hallmark of a symmetry-breaking self-organization process. Healing of localized wounds in Characean cells also furnishes evidence, where the actin network regenerates in a gradually organizing process (31, 32). Even *ex vivo* experiments lend credence to such a theory: cytoplasmic droplets forcibly extracted from *Chara* cells can begin spontaneously circulating at a steady rate (8, 33, 34) likely owing to a self-organizing process (35). Furthermore, images of filament networks in very young Characean cells show long cables forming only after elongation begins, with just a disorderly meshwork at genesis (36).

In this work, we will unify this wealth of experimental evidence for a self-organization mechanism by constructing a simple theoretical model of streaming emergence during cell development. The model will couple the hydrodynamics of the cytoplasm with the dynamics of a microfilament suspension subject to a few key reorienting and organizing effects. We will then illustrate the model’s capacity for mimicking the emergence of Characean

Author contributions: F.G.W. and R.E.G. designed research, performed research, and wrote the paper.

The authors declare no conflict of interest.

This article is a PNAS Direct Submission.

Freely available online through the PNAS open access option.

<sup>1</sup>To whom correspondence should be addressed. E-mail: r.e.goldstein@damtp.cam.ac.uk.

This article contains supporting information online at [www.pnas.org/lookup/suppl/doi:10.1073/pnas.1302736110/-DCSupplemental](http://www.pnas.org/lookup/suppl/doi:10.1073/pnas.1302736110/-DCSupplemental).

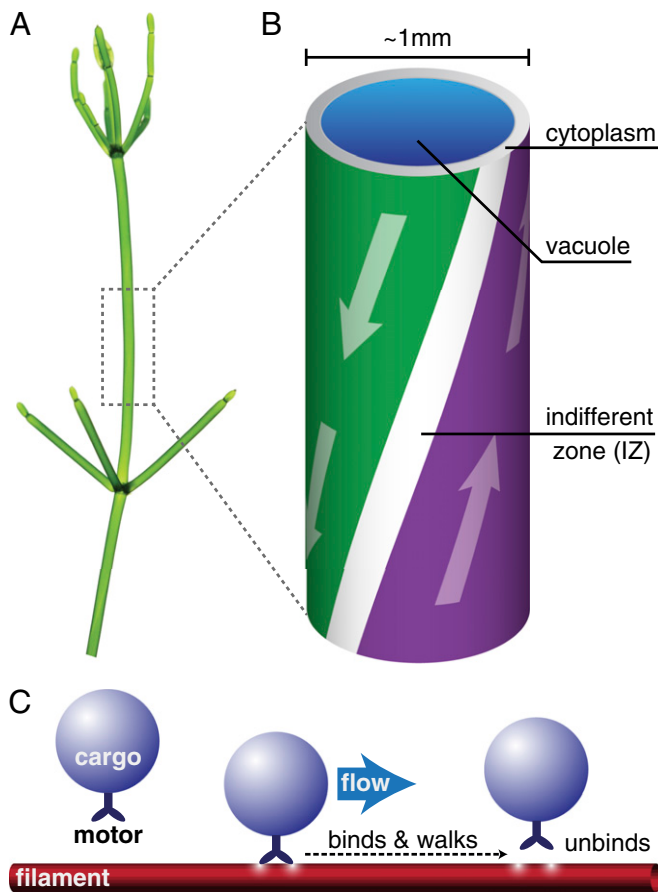


**Fig. 1.** Cytoplasmic streaming in *Chara corallina*. (A) Internodes and branchlets of *Chara*. Individual internodes can grow up to 10 cm long. (B) Rotational streaming in a single internodal cell of *Chara*. The stripes indicate the polarity of actin cables at the periphery driving flow in the cytoplasm and vacuole. (C) Microscopic mechanism driving plant cell streaming. Cargo-carrying myosin motors bind to actin filaments and entrain flow as they walk.

streaming by way of an example and a parameter space scan to identify regimes of robust cyclosis development. Finally, we will discuss the model in the context of pathologies and disruptions to understand the importance of each of the components of the filament dynamics.

**Model**

A young *Chara* cell is modeled as a cylinder of radius  $R$  with periodic boundaries at a distance  $L$  apart. The fixed chloroplasts lie at the edge, with the subcortical cytoplasm a thin cylindrical layer between the chloroplasts and the vacuolar membrane; the vacuole then comprises the bulk of the cell. The cytoplasm is taken to consist of a layer of short, initially disordered actin filaments beneath a layer of myosin-coated endoplasmic reticulum vesicles, which drive flow by forcing the cytoplasm as they process on the actin filaments (Fig. 1C). Because the subcortical layer is very thin compared with the vacuole, we approximate the cytoplasmic layer as a purely 2D cylindrical shell. We also assume that the effective viscosity contrast between cytoplasm and vacuolar fluid is sufficiently large to take vacuolar flow as purely passive, induced by cytoplasmic flow (25) but not affecting it. This yields a truly 2D problem.

Our final simplification is to neglect the helical twist in the streaming pattern (Fig. 1B). No discernible twist exists in young cells with developed actin cables (28), so its appearance is more likely connected to later development of the microtubule

cytoskeleton (37) by a process of twisting growth once the main cables are established and bound to the cortical chloroplasts (38). The twist appears to be advantageous primarily for large, mature cells, where it enhances vacuolar mixing and nutrient uptake (25, 26).

We will now formalize the hydrodynamics. Endow the shell with cylindrical coordinates  $(\theta, z)$  and corresponding unit vectors  $\mathbf{e}_\theta, \mathbf{e}_z$ . Let  $\mathbf{u}(\mathbf{x})$  be the velocity field of the suspending cytoplasmic fluid. The small velocity of streaming allows us to work in the zero Reynolds number limit. We then take  $\mathbf{u}$  to obey the forced Stokes equations with friction,

$$-\mu \nabla^2 \mathbf{u} + \nu \mathbf{u} + \nabla \Pi = \mathbf{F},$$

where  $\Pi(\mathbf{x})$  is the 2D pressure and  $\mathbf{F}(\mathbf{x})$  is the filament-induced forcing, discussed shortly. The frictional term  $\nu \mathbf{u}$  captures the effect of the no-slip boundary proximity in our thin-shell approximation, in a manner similar to Hele–Shaw flow (SI Text).

There are two crucial constraints on the flow field that must be incorporated. First, because the tonoplast membrane, which separates the cytoplasm and vacuole, behaves as a 2D incompressible fluid (39), we must have incompressibility  $\nabla \cdot \mathbf{u} = 0$ . Second, the presence of end caps on the cell must be acknowledged, either through explicit modeling of the end geometry or, as we do here, qualitatively through the simple extra constraint of zero net flux  $\int_0^{2\pi} \int_0^L \mathbf{u} \cdot \mathbf{e}_z \, dz d\theta = 0$ , essentially due to the incompressibility of a finite domain in the  $\mathbf{e}_z$  direction. This is balanced by allowing a longitudinal pressure gradient  $\Pi_0$  and writing  $\Pi(\mathbf{x}) = \Pi_0 z + \Pi'(\mathbf{x})$ , with  $\Pi'(\mathbf{x})$  the remaining fully periodic pressure field.

We now turn to the filament suspension, whose dynamics will incorporate several crucial effects. The filaments are taken to be restricted: passive advection and shear alignment in the flow  $\mathbf{u}$  is inhibited by a factor  $\epsilon$  due to frictional or binding effects of the filaments on the chloroplasts or with cortical polymer networks. As a consequence of restriction, the filaments are non-self-advective: a vesicle walking forward on a filament will induce only a negligible backward propulsion of the filament itself. The filaments are also taken to spontaneously bundle: filaments will locally align with each other, controlled by a coupling constant  $\alpha_p$  (a rate constant for the exponential growth of small local polarization), mimicking the presence of bundling proteins. (Inhibiting the action of bundling proteins thus corresponds to setting  $\alpha_p = 0$ .)

To represent nonspherical cellular geometry or substrate patterning we include a repulsive direction  $\mathbf{d}$ , which filaments will preferentially avoid, with coupling constant  $\kappa$  (Fig. 3A); this will be set here to  $\mathbf{d} = \mathbf{e}_\theta$ , the circumferential direction. Although apparently a strong assumption, there is remarkable experimental precedent for such an effect whereby filaments can reorient circumferentially around cells upon inhibition of binding or director components (40–42).

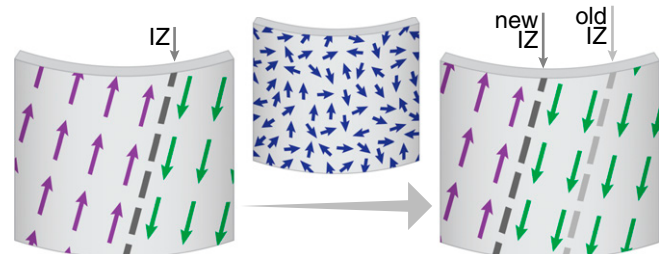


**Fig. 2.** Disruption, rearrangement, and resumption of streaming in *Chara* (28). Filament bundles disorganize and reform with the IZ in a new location.

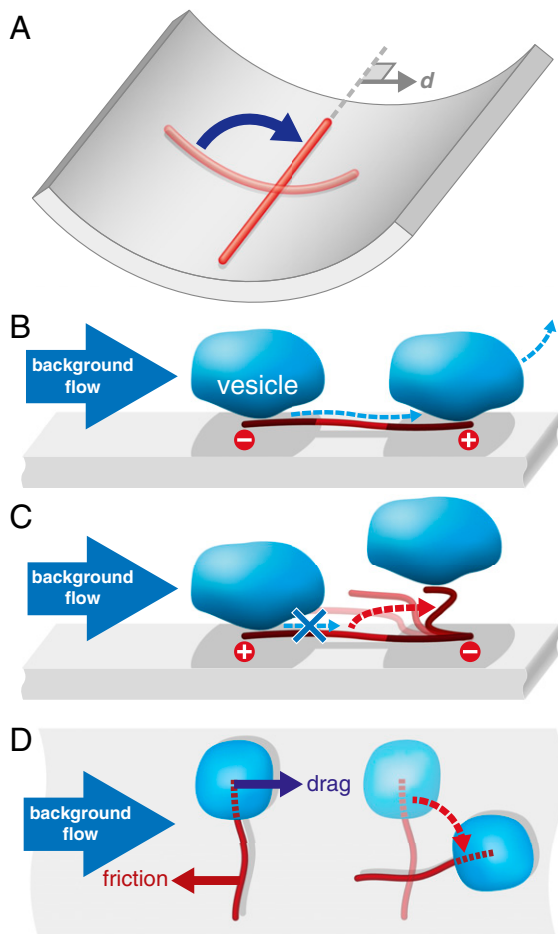


**Fig. 3.** Filament reorganization mechanisms. (A) Repulsive direction: a filament preferentially reorients away from a direction  $\mathbf{d}$  either to minimize physical curvature or minimize interactions. (B–D) Polar flow reorientation: rather than aligning nematicly with flow shear, filaments can align in a polar fashion with flow itself. Alignment with the plus end downstream is stable (B), but hydrodynamic drag on vesicles bound to the filament competes with friction from wall restriction when the motor is not free to walk downstream (C and D).

In the absence of any other contributing factors, the effects described above will tend to produce a uniformly polarized suspension in a direction perpendicular to  $\mathbf{d}$ . There is one more key factor: polar flow alignment, with coupling constant  $\alpha_u$  (encoding the linear growth rate of filament polarization with cytoplasm flow, similar to  $\alpha_p$ ). We argue that the presence of myosin-coated vesicles brings about alignment of the filaments with the flow field  $\mathbf{u}$  itself in a truly polar fashion, minus end upstream and plus end downstream, supplementing traditional nematic alignment with flow shear  $\nabla\mathbf{u}$ . Suppose that a motor-laden vesicle approaches a filament, advected by a net background flow  $\mathbf{u}$  from the action of other vesicles processing along filaments nearby. There are then three basic cases to consider for the filament orientation relative to the flow. If the vesicle approaches a microfilament oriented parallel with  $\mathbf{u}$ —that is, minus end upstream so the myosin walk direction is with the flow—then the vesicle can bind, process along the filament at a speed  $\sim|\mathbf{u}|$ , and unbind with little change to the filament (Fig. 3B). This implies parallel flow alignment is stable. Antiparallel alignment, with plus end upstream and walk direction against the flow, is unstable: a vesicle bound upstream on the filament will be impeded from walking by hydrodynamic drag, stall on

the restricted filament, and twist it into the flow (Fig. 3C). Finally, perpendicular alignment induces reorientation either parallel or antiparallel to the flow upon binding of a vesicle, because a torque is generated by the competition of filament restriction against hydrodynamic drag (Fig. 3D). This effect is not unique to microfilaments: thin-film dumbbell microswimmers are subject to the same polar alignment, driven by asymmetric friction forces (43).

For this reorientation mechanism to occur and be robust (that is, stable when oriented parallel with the flow), there are two important conditions. First, the timescale  $\tau_r$  for filament reorientation must be shorter than the timescale  $\tau_d$  for motor detachment after stalling (44) in order for any appreciable filament reorientation to occur in the flow-antiparallel and flow-perpendicular cases. Second, the timescale  $\tau_p$  for a motor to process along a flow-parallel filament must be shorter than the filament reorientation timescale  $\tau_r$ , in order for orientation parallel with the flow to be stable; if this is not the case, then no orientation is stable, and the filament will writhe continuously over time irrespective of its orientation relative to the background flow. Thus, we require  $\tau_p \ll \tau_r \ll \tau_d$ . The sliding speed  $\sim 100 \mu\text{m/s}$  (45) on  $\sim 10 \mu\text{m}$  filaments yields a quick procession timescale  $\tau_p \sim 10^{-1} \text{ s}$ . By contrast, it has been suggested that the very fast streaming may in fact be due to the action of many nonprocessive motors on one vesicle acting simultaneously (45, 46), which would likely yield a long stall detachment time  $\tau_d > 1 \text{ s}$  due to the long dwell time of individual characean myosins (46). Microfluidic studies indicate that the reorientation timescale  $\tau_r$  lies in-between these two extremes (47), indicating that this reorientation mechanism is indeed viable.

To describe the microfilaments we use a formalism from the theory of active suspensions (35, 48). The full derivation of the dynamics can be found in *SI Text*; we summarize it here, as follows. At each point  $\mathbf{x}$  on the cylinder, define the angular distribution function  $\Psi(\mathbf{x}, \mathbf{p})$  of microfilaments with unit direction  $\mathbf{p}$ . From this, we define the local filament concentration  $c(\mathbf{x}) = \int_{\mathbf{p}} \Psi(\mathbf{x}, \mathbf{p}) d\mathbf{p}$  and average orientation director  $\mathbf{P}(\mathbf{x}) = c(\mathbf{x})^{-1} \int_{\mathbf{p}} \mathbf{p} \Psi(\mathbf{x}, \mathbf{p}) d\mathbf{p}$ . The distribution  $\Psi(\mathbf{x}, \mathbf{p})$  obeys a Smoluchowski equation, whose orientational moments yield the dynamics of the concentration and director fields after applying a simple moment closure approximation, whose viability is discussed further in *SI Text*. Our non-self-advective supposition then reduces the concentration dynamics to pure advection-diffusion (*SI Text*), allowing us to neglect fluctuations and reduce to a uniform concentration  $c(\mathbf{x}) \equiv c_0$ .

The system is closed by defining the flow forcing  $\mathbf{F}(\mathbf{x})$ . As the filaments are restricted by frictional forces with the outer wall, the primary contribution of a vesicle processing along a filament is a point force (i.e., a Stokeslet), suggesting a simple relationship  $\mathbf{F} \propto \mathbf{P}$ . However, global streaming does not persist in the presence of filament unbundling agents, whereas the actin–myosin interaction remains uninhibited (28). Therefore, the flow does not play a role in the linear stability of a disordered suspension, implying that the force must be nonlinear in the local alignment  $\mathbf{P}$  (*SI Text*). We take the lowest nonlinear order permitted by symmetry and write  $\mathbf{F} = \Phi |\mathbf{P}|^2 \mathbf{P}$ . The proportionality constant  $\Phi$  encodes the force per unit area generated by vesicles processing along perfectly aligned filaments, and thus includes all information relating to vesicle number, procession speed, and binding rates.

The last step is to nondimensionalize all variables and coupling constants; we scale space by the radius  $R$  and choose rescalings to eliminate the friction coefficient  $\nu$  and the forcing constant  $\Phi$  (*SI Text*). The final dynamics for  $\mathbf{P}$  read





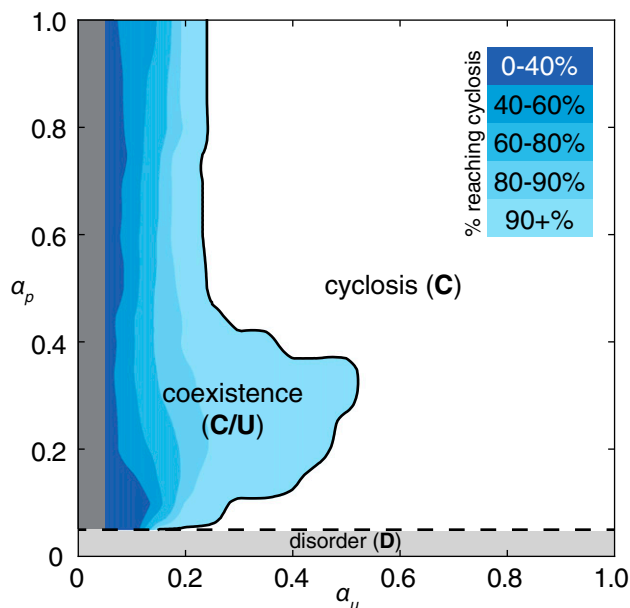


**Fig. 5.** Results of a numerical parameter sweep over  $\alpha_p$  and  $\alpha_u$  between 0.025 and 1, with other parameters held fixed as in the text. The entire set of  $20 \times 20$  parameters was simulated for 50 different random initial conditions, uncovering regions of cyclosis/unidirectional bistability (C/U) and fully robust cyclosis (C). Color coding in region C/U denotes the percentage of the initial conditions that developed into steady cyclosis states at each pair of parameters. Region D, where  $\alpha_p < d^{(l)}$ , is linearly stable and develops no streaming.

three distinct regimes (Fig. 5): disorder (D), cyclosis/unidirectional coexistence (C/U), and full cyclosis (C). Parameters in region D have  $\alpha_p$  too low for spontaneous order to flourish, where the disordered state  $\mathbf{P} = \mathbf{0}$  is linearly stable. In region C/U, the system may evolve into either the cyclosis state or the unidirectional state  $\mathbf{P} = P_0 \mathbf{e}_z$  (where  $P_0$  is a constant). Which steady state is reached is dependent on the precise nature of the initial conditions, a consequence of coexistence of basins of attraction in the neighborhood of the Fourier space origin. Parameters in region C always developed the desired cyclosis solutions for all sets of initial conditions, indicating that the basin of attraction of the unidirectional state is now negligible. These regimes can be understood further by considering the simplified one-dimensional regime of  $z$ -independent and  $z$ -parallel alignment, i.e.,  $\mathbf{P} = P(\theta) \mathbf{e}_z$  (SI Text).

**Flow-Stabilized Pattern Formation.** The one-dimensional simplification also allows us to consider the model in the context of pattern formation theory. When  $\alpha_u = 0$ , the system assumes nonconservative Allen–Cahn form, for which it can be shown that a spatially oscillating state is always unstable; consequently, fronts separating regions of upward and downward alignment will always eventually coalesce (49). However,  $\alpha_u > 0$  introduces a difficult nonlocal term, which cannot be written as the gradient of some free energy functional. In fact, for  $\alpha_u$  above a small threshold, cyclosis solutions are stabilized by global flow alignment effects. The exact threshold as a function of  $\alpha_p$  can be determined by fixing  $\alpha_p$  and varying  $\alpha_u$  to compute trajectories of eigenvalues of the nonlocal Sturm–Liouville problem induced by linear stability analysis. This is discussed further in SI Text.

## Discussion

We have demonstrated the capability of this model for simulating the emergence of Characean streaming. For the computational

study, we focused on the roles of the polarization and flow-coupling constants  $\alpha_p$  and  $\alpha_u$ . Perhaps the next most important parameter is the directional repulsion  $\kappa$ , which we have not investigated in detail here. The value we chose,  $\kappa = 0.5$ , is a nice intermediate providing a definite preference for upward orientation, but not so strong as to completely dominate the early-time dynamics. However, if  $\kappa$  is too small, then little or no directional effects are felt, and the dynamics may be either unsteady or settle into circumferential flows.

In fact, studies of poor, malformed streaming induced in vivo hint at the true effects of removing directional preference. Conversely, a suitable model for streaming should be able to reproduce observed pathologies and experimental disruptions, at least qualitatively, and it is these we now briefly discuss. Total cable fragmentation (28, 30, 50) has already been mentioned and directly corresponds to setting  $\alpha_p = 0$  to inhibit bundling effects. There is also the possibility of atypical reorganization of the actin cables; to our knowledge, such behavior has not yet been induced in Characean cells. Nevertheless, it has been documented in other types of orderly streaming plant cells, with which a direct comparison can be made owing to the generality of this approach. On inhibiting the binding of the cell membrane to the cell wall, actin cables in *Vallisneria* mesophyll cells can reorient from longitudinal to circumferential, running around the long axis (40). Similar reorientation can be induced in *Lilium* pollen tubes, where actin cables reorient circumferentially in regions lacking longitudinal microtubules (41). Both studies supply evidence for the restriction and repulsive direction components of our model. Even though these atypical streaming arrangements were not induced during cell development, such a configuration can be reproduced by choosing parameters appropriately (SI Text).

We have considered the bases of  $\alpha_p$  (bundling),  $\kappa$  (geometric reorientation), and  $\epsilon$  (restriction), but how might one experimentally account for the polar alignment coefficient  $\alpha_u$ ? Setting  $\alpha_u \approx 0$  corresponds to inhibiting the ability of myosin to walk on actin. In the Characeae, one would also have to disorganize the filament network (28) to observe its effect from a base state. We would then expect a unidirectional streaming pattern to emerge, or at least a metastable cyclosis with unequal widths of opposing streams, as the filaments bundle. Such an experiment would be an exciting test of the principal ideas on which this conceptually simple yet powerful self-organization model has been built.

## Materials and Methods

**Simulation Method.** Simulations were performed using spectral methods, evaluating gradients and evolving in time in Fourier space and moving into physical space to evaluate nonlinearities. The periodic boundary conditions were then implicit in choosing a Fourier basis. Explicit fourth-order Runge–Kutta integration was used for time evolution.

**Initial Conditions.** For all simulations, the initial conditions were of total filament disorder as follows. Suppose in a small area  $dA$  there are  $N \gg 1$  filaments whose orientations  $\mathbf{P}_i$ ,  $1 \leq i \leq N$ , are uniformly distributed, i.e.,  $\mathbf{P}_i = (\cos \theta_i, \sin \theta_i)$ , where  $\theta_i \sim \mathcal{U}(0, 2\pi)$ . Then because the  $\{\theta_i\}$  are independent and identically distributed random variables, the central limit theorem applies to  $\mathbf{P} = \frac{1}{N} \sum_i \mathbf{P}_i$ , giving that  $P_\theta, P_z \sim \mathcal{N}(\mu, \sigma^2/N)$  with  $\mu = \mathbb{E}(\cos \theta_i) = \mathbb{E}(\sin \theta_i) = 0$  and  $\sigma^2 = \text{Var}(\cos \theta_i) = \text{Var}(\sin \theta_i) = 1/2$ . Therefore, to model an initial distribution of  $N \gg 1$  filaments per grid square, initial conditions are drawn as  $P_\theta, P_z \sim \mathcal{N}(0, \frac{1}{2N})$ .  $N = 1,000$  was taken for all simulations.

**ACKNOWLEDGMENTS.** We thank J. Dunkel, A. Honerkamp-Smith, P. Khuc Trong, M. Polin, and H. Wioland for discussions. This work was supported by the Engineering and Physical Sciences Research Council and European Research Council Advanced Investigator Grant 247333.

1. Khuc Trong P, Guck J, Goldstein RE (2012) Coupling of active motion and advection shapes intracellular cargo transport. *Phys Rev Lett* 109(2):028104.
2. Ganguly S, Williams LS, Palacios IM, Goldstein RE (2012) Cytoplasmic streaming in *Drosophila* oocytes varies with kinesin activity and correlates with the microtubule cytoskeleton architecture. *Proc Natl Acad Sci USA* 109(38):15109–15114.
3. Goehring NW, et al. (2011) Polarization of PAR proteins by advective triggering of a pattern-forming system. *Science* 334(6059):1137–1141.
4. Allen NS, Allen RD (1978) Cytoplasmic streaming in green plants. *Annu Rev Biophys Bioeng* 7:497–526.
5. Taylor LP, Hepler PK (1997) Pollen germination and tube growth. *Annu Rev Plant Physiol Plant Mol Biol* 48:461–491.
6. Hepler PK, Vidali L, Cheung AY (2001) Polarized cell growth in higher plants. *Annu Rev Cell Dev Biol* 17:159–187.
7. Howard J, Grill SW, Bois JS (2011) Turing's next steps: The mechanochemical basis of morphogenesis. *Nat Rev Mol Cell Biol* 12(6):392–398.
8. Kamiya N (1959) *Protoplasmic Streaming* (Springer, Vienna).
9. Kruse K, Joanny JF, Jülicher F, Prost J, Sekimoto K (2004) Asters, vortices, and rotating spirals in active gels of polar filaments. *Phys Rev Lett* 92(7):078101.
10. Allard JF, Wasteneys GO, Cyttrynbaum EN (2010) Mechanisms of self-organization of cortical microtubules in plants revealed by computational simulations. *Mol Biol Cell* 21(2):278–286.
11. Surrey T, Nédélec F, Leibler S, Karsenti E (2001) Physical properties determining self-organization of motors and microtubules. *Science* 292(5519):1167–1171.
12. Narayan V, Ramaswamy S, Menon N (2007) Long-lived giant number fluctuations in a swarming granular nematic. *Science* 317(5834):105–108.
13. Schaller V, Weber C, Semmrich C, Frey E, Bausch AR (2010) Polar patterns of driven filaments. *Nature* 467(7311):73–77.
14. Sanchez T, Chen DTN, DeCamp SJ, Heymann M, Dogic Z (2012) Spontaneous motion in hierarchically assembled active matter. *Nature* 491(7424):431–434.
15. Zumdick A, et al. (2005) Continuum description of the cytoskeleton: Ring formation in the cell cortex. *Phys Rev Lett* 95(25):258103.
16. Srivastava P, Shlomovitz R, Gov NS, Rao M (2013) Patterning of polar active filaments on a tense cylindrical membrane. *Phys Rev Lett* 110(16):168104.
17. Corti B (1774) *Osservazione Microscopiche sulla Tremella e sulla Circolazione del Fluido in una Pianta Acquajiuola* (Appresso Giuseppe Rocchi, Lucca, Italy).
18. Nothnagel EA, Webb WW (1982) Hydrodynamic models of viscous coupling between motile myosin and endoplasm in characean algae. *J Cell Biol* 94(2):444–454.
19. Kachar B, Reese TS (1988) The mechanism of cytoplasmic streaming in characean algal cells: Sliding of endoplasmic reticulum along actin filaments. *J Cell Biol* 106(5):1545–1552.
20. Williamson RE (1993) Organelle movements. *Annu Rev Plant Biol* 44:181–202.
21. Sheetz MP, Spudis JA (1983) Movement of myosin-coated fluorescent beads on actin cables in vitro. *Nature* 303(5912):31–35.
22. Shimmen T (2007) The sliding theory of cytoplasmic streaming: Fifty years of progress. *J Plant Res* 120(1):31–43.
23. Kersey YM, Hepler PK, Palevitz BA, Wessells NK (1976) Polarity of actin filaments in Characean algae. *Proc Natl Acad Sci USA* 73(1):165–167.
24. Kersey YM, Wessells NK (1976) Localization of actin filaments in internodal cells of characean algae. A scanning and transmission electron microscope study. *J Cell Biol* 68(2):264–275.
25. Goldstein RE, Tuval I, van de Meent JW (2008) Microfluidics of cytoplasmic streaming and its implications for intracellular transport. *Proc Natl Acad Sci USA* 105(10):3663–3667.
26. van de Meent JW, Tuval I, Goldstein RE (2008) Nature's microfluidic transporter: Rotational cytoplasmic streaming at high Péclet numbers. *Phys Rev Lett* 101(17):178102.
27. van de Meent JW, Sederman AJ, Gladden LF, Goldstein RE (2010) Measurement of cytoplasmic streaming in single plant cells by magnetic resonance velocimetry. *J Fluid Mech* 642:5–14.
28. Foissner I, Wasteneys GO (2000) Microtubule disassembly enhances reversible cytochalasin-dependent disruption of actin bundles in characean internodes. *Protoplasma* 214(1-2):33–44.
29. Jarosch R (1956) Die Impulsrichtungsänderungen bei der Induktion der Protoplasmaströmung. *Protoplasma* 47(3-4):478–486.
30. Ryu JH, Takagi S, Nagai R (1995) Stationary organization of the actin cytoskeleton in *Vallisneria*: The role of stable microfilaments at the end walls. *J Cell Sci* 108(Pt 4):1531–1539.
31. Foissner I, Lichtscheidl IK, Wasteneys GO (1996) Actin-based vesicle dynamics and exocytosis during wound wall formation in characean internodal cells. *Cell Motil Cytoskeleton* 35(1):35–48.
32. Foissner I, Wasteneys GO (1997) A cytochalasin-sensitive actin filament meshwork is a prerequisite for local wound wall deposition in *Nitella* internodal cells. *Protoplasma* 200(1-2):17–30.
33. Yotsuyanagi Y (1953) Recherches sur les phénomènes moteurs dans les fragments de protoplasme isolés. I. Mouvement rotatoire et le processus de son apparition. *Cytologia (Tokyo)* 18(2):146–156.
34. Yotsuyanagi Y (1953) Recherches sur les phénomènes moteurs dans les fragments de protoplasme isolés. II. Mouvements divers déterminés par la condition de milieu. *Cytologia (Tokyo)* 18(3):202–217.
35. Woodhouse FG, Goldstein RE (2012) Spontaneous circulation of confined active suspensions. *Phys Rev Lett* 109(16):168105.
36. Wasteneys GO, Collings DA, Gunning BE, Hepler PK, Menzel D (1996) Actin in living and fixed characean internodal cells: Identification of a cortical array of fine actin strands and chloroplast actin rings. *Protoplasma* 190(1-2):25–38.
37. Green PB (1962) Mechanism for plant cellular morphogenesis. *Science* 138(3548):1404–1405.
38. Green PB (1954) The spiral growth pattern of the cell wall in *Nitella axillaris*. *Am J Bot* 41(5):403–409.
39. Woodhouse FG, Goldstein RE (2012) Shear-driven circulation patterns in lipid membrane vesicles. *J Fluid Mech* 705:165–175.
40. Masuda Y, Takagi S, Nagai R (1991) Protease-sensitive anchoring of microfilament bundles provides tracks for cytoplasmic streaming in *Vallisneria*. *Protoplasma* 162(2-3):151–159.
41. Foissner I, Obermeyer G (2002) Reversible protein phosphorylation regulates the dynamic organization of the pollen tube cytoskeleton: Effects of calyculin A and okadaic acid. *Protoplasma* 220(1-2):1–15.
42. Tominaga M, Morita K, Sonobe S, Yokota E, Shimmen T (1997) Microtubules regulate the organization of actin filaments at the cortical region in root hair cells of *Hydrocharis*. *Protoplasma* 199(1-2):83–92.
43. Brotto T, Caussin JB, Lauga E, Bartolo D (2013) Hydrodynamics of confined active fluids. *Phys Rev Lett* 110(3):038101.
44. Parmeggiani A, Jülicher F, Peliti L, Prost J (2001) Detachment of molecular motors under tangential loading. *Europhys Lett* 56(4):603–609.
45. Shimmen T, Yokota E (2004) Cytoplasmic streaming in plants. *Curr Opin Cell Biol* 16(1):68–72.
46. Kimura Y, Toyoshima N, Hirakawa N, Okamoto K, Ishijima A (2003) A kinetic mechanism for the fast movement of *Chara* myosin. *J Mol Biol* 328(4):939–950.
47. Kantsler V, Goldstein RE (2012) Fluctuations, dynamics, and the stretch-coil transition of single actin filaments in extensional flows. *Phys Rev Lett* 108(3):038103.
48. Saintillan D, Shelley MJ (2008) Instabilities, pattern formation, and mixing in active suspensions. *Phys Fluids* 20(12):123304.
49. Pismen LM (2006) *Patterns and Interfaces in Dissipative Dynamics* (Springer, Berlin).
50. Foissner I, Wasteneys GO (2007) Wide-ranging effects of eight cytochalasins and lantrunculin A and B on intracellular motility and actin filament reorganization in characean internodal cells. *Plant Cell Physiol* 48(4):585–597.